Molecular dynamics simulation of backflow generation in nematic liquid crystals

Alfeus Sunarso,[a] Tomohiro Tsuji, and Shigeomi Chono
Department of Mechanical Engineering, Kochi University of Technology, Kami-shi, Kochi 782-8502, Japan

(Received 14 August 2008; accepted 24 November 2008; published online 18 December 2008)

The mechanism of backflow generation in nematic liquid crystals under the application of an electric field is investigated by molecular dynamics simulation, and the roles of intermolecular interaction in the generation of bulk velocity are investigated. It is confirmed that the reorientation of molecules by the application of an electromagnetic field induces a transient "S-shaped" bulk velocity profile. The rotation and rearrangement of molecules during the reorientation process generate a local bulk velocity gradient. © *2008 American Institute of Physics*. [DOI: 10.1063/1.3050111]

Liquid crystals exhibit many features that are interesting from technical and scientific viewpoints. The ability to control their molecular orientation by the application of an electric field has led to the development of liquid crystal displays (LCDs). Research in this field has driven the large-scale production of LCDs. As LCD technology has been established, the development of different applications of liquid crystals has attracted growing attention. Recently, the potential development of a liquid-crystal-based microactuator or manipulator has been proposed.[1,2] The basic idea is to employ the flow induced by an electric field to control the motion of an object. The induced flow is known as backflow.

Early studies on backflow dealt with its effects on the switching process.[3–5] In more recent studies, the potential application of backflow for controlling the motion of an object has been addressed.[1,2] The backflow has been studied mainly in terms of the Ericksen–Leslie macroscopic continuum theory.[6–8] There are also different methods to study the effect of backflow such as the method used in Ref. 9, where the Lattice–Boltzmann simulation was used to solve the Beris-Edwards equations.[10] In Ref. 1, the continuum level mechanism of backflow has been proposed. However, to understand the detailed mechanism at the molecular level, further investigation is required. In the present work, we study the mechanism by molecular dynamics simulation. The roles of intermolecular interaction in the generation of bulk velocity are investigated.

We consider the dynamics of a nematic liquid crystal confined between parallel plates. The computational domain and molecular model are shown in Fig. 1. The liquid crystal molecules are represented as ellipsoids. Without the electric field effect, the molecules interact through the Gay–Berne potential.[11]

$$\phi_{ij}^{\mathrm{GB}} = 4\varepsilon(\hat{\boldsymbol{u}}_i,\hat{\boldsymbol{u}}_i,\hat{\boldsymbol{r}}_{ij})\left\{\left[\frac{\sigma_0}{r_{ij}-\sigma(\hat{\boldsymbol{u}}_i,\hat{\boldsymbol{u}}_i,\hat{\boldsymbol{r}}_{ij})+\sigma_0}\right]^{12} - \left[\frac{\sigma_0}{r_{ij}-\sigma(\hat{\boldsymbol{u}}_i,\hat{\boldsymbol{u}}_i,\hat{\boldsymbol{r}}_{ij})+\sigma_0}\right]^{6}\right\}. \tag{1}$$

Here, $\hat{\boldsymbol{u}}_i$ and $\hat{\boldsymbol{u}}_j$ are unit vectors representing the orientation of molecules i and j, respectively, and $\hat{\boldsymbol{r}}_{ij}$ is the unit vector of vector $\boldsymbol{r}_{ij}$ ($\hat{\boldsymbol{r}}_{ij}=\boldsymbol{r}_{ij}/r_{ij}$) that connects the centers of mass of molecules i and j. $\sigma(\hat{\boldsymbol{u}}_i,\hat{\boldsymbol{u}}_i,\hat{\boldsymbol{r}}_{ij})$ represents the contribution of molecular orientation on the intermolecular distance, while $\varepsilon(\hat{\boldsymbol{u}}_i,\hat{\boldsymbol{u}}_i,\hat{\boldsymbol{r}}_{ij})$ defines the potential well. The parameters of the potential (related to $\sigma(\hat{\boldsymbol{u}}_i,\hat{\boldsymbol{u}}_i,\hat{\boldsymbol{r}}_{ij})$ and $\varepsilon(\hat{\boldsymbol{u}}_i,\hat{\boldsymbol{u}}_i,\hat{\boldsymbol{r}}_{ij})$) are molecular length scale σ_0, energy scale ε_0, molecular aspect ratio σ_r, energy ratio ε_r, and the constants for the potential well μ and ν.

To account for the effect of electric field, we use a similar approach as used in Refs. 12 and 13, in which the electric field induced molecular torque is considered as the contribution of the induced polarization. The application of an electric field $\boldsymbol{E}=E\hat{\boldsymbol{e}}$ induces an electric dipole $\boldsymbol{p}$ on each molecule, $\boldsymbol{p}=\alpha E(\hat{\boldsymbol{e}}\cdot\hat{\boldsymbol{u}})\hat{\boldsymbol{u}}$, where α is the polarisability, and E and $\hat{\boldsymbol{e}}$ are the strength and unit vector of the electric field, respectively. The induced dipole contributes to the molecular interaction through a dipole-dipole interaction potential Ref. 14.

$$\phi_{ij}^{\mathrm{DP}} = \frac{1}{r_{ij}^3}\{\boldsymbol{p}_i\cdot\boldsymbol{p}_j - 3(\boldsymbol{p}_i\cdot\hat{\boldsymbol{r}}_{ij})(\boldsymbol{p}_j\cdot\hat{\boldsymbol{r}}_{ij})\}. \tag{2}$$

Furthermore, the interaction between the electric field and the induced dipoles generates a torque $\boldsymbol{T}$ on each molecule,

$$\boldsymbol{T}_i = \boldsymbol{p}_i\times\boldsymbol{E} = \alpha E^2(\hat{\boldsymbol{e}}\cdot\hat{\boldsymbol{u}}_i)(\hat{\boldsymbol{u}}_i\times\hat{\boldsymbol{e}}). \tag{3}$$

Therefore, equations of motion of each molecule i are as follows:

$$m_i\frac{d^2\boldsymbol{r}_i}{dt^2} = -\sum_{j=0,j\neq i}^{N}\left(\frac{\partial\phi_{ij}}{\partial\boldsymbol{r}_{ij}}\right), \tag{4}$$

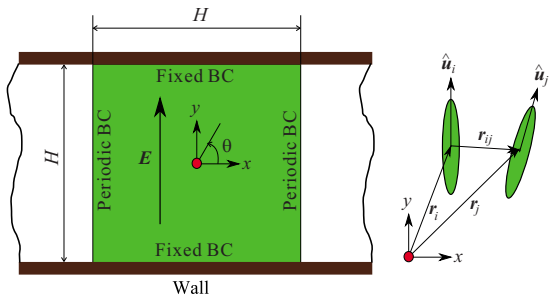

FIG. 1. (Color online) Computational domain and molecular model.

[a]Electronic mail: sunarso@kochi-tech.ac.jp.

$$I_i \frac{d^2\theta_i}{dt^2} = -\sum_{j=0,j\neq i}^{N} \left(\hat{\boldsymbol{u}}_i \times \frac{\partial \phi_{ij}}{\partial \hat{\boldsymbol{u}}_i} \right) + T_i. \quad (5)$$

Here, the potential ϕ_{ij} is the sum of the Gay–Berne potential and the dipole-dipole potential, $\phi_{ij}=\phi_{ij}^{\mathrm{GB}}+\phi_{ij}^{\mathrm{DP}}$. m and I are the mass and moment of inertia of a molecule, respectively, and N is the number of molecules.

Equations (4) and (5) are solved in the dimensionless forms, and variables such as position y, number density ρ, temperature T, and time t are expressed in the dimensionless forms: $y^*=y/\sigma_0$, $\rho^*=\rho/\sigma_0^3$, $T^*=k_BT/\varepsilon_0$ and $t^*=[(\varepsilon_0/m)^{1/2}/\sigma_0]t$. The parameters of the Gay–Berne potential are $\nu=1$, $\mu=2$, $\epsilon_r=1$, and $\sigma_r=5$. This set of parameters results in a stable nematic phase over a relatively wide range of temperature and number density. It should be noted that ϕ_{ij}^{GB} is a short range interaction, while ϕ_{ij}^{DP} is a long range interaction that requires special treatment. We used the reaction field method,[14] and set the cutoff radius to $r_c^*=20$.

The results reported here were computed using an ensemble of 10 000 molecules with $T^*=1$, $\rho^*=0.188$ and $\lambda^*=\alpha E^2/\varepsilon_0=2$. The size of simulation box is $H=230\sigma_0$, where σ_0 is the length scale of molecular diameter, which is in the order of subnanometer for molecules of liquid crystals. The size of simulation box is one to two order smaller than the size of cells used in experimental study of backflow, and therefore we do not make any quantitative comparisons with experimental results. However, the results of the simulation should give a qualitative explanation on the roles of intermolecular interactions in the generation of macroscopic flow.

To obtain an initial configuration, the molecules were initially arranged with uniform spacing and orientation, and then simulation of the ensemble at constant temperature was performed in a 40 000 iterations ($t^*=200$), which was a sufficient number to obtain a steady nematic phase. The temperature was controlled using the Nose–Hoover thermostat. The simulation of backflow was started using the obtained initial configuration with a random initial velocity. To equilibrate the random velocity, the simulation was initialized using the temperature controlled ensemble for a few iterations ($t^*=1$), before the electric field was imposed. To ensure that the dynamics of the molecules follows the pure Newtonian dynamics without any artificial terms arise from temperature control method, after the electric field was imposed, the temperature control was disabled. As shown in Fig. 1, a periodic boundary condition was set at the left and right boundaries. At the upper and lower boundaries, layers of molecules with fixed position and orientation with pretilt angle of 30° were introduced to account for the wall anchoring effect. The pretilt angle is set to a relatively large value to reduce the computation time.

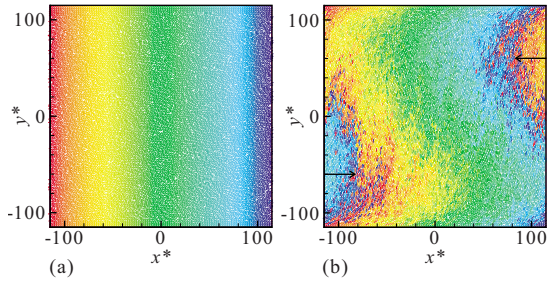

FIG. 2. (Color online) Snapshot of molecules at equilibrium (a) and after application of electric field for time $t^*=1000$ (b).

Snapshots of molecules at equilibrium and after the application of an electric field are shown in Fig. 2. The colors represent the initial horizontal position x^* of each molecule. It can be observed that after the application of the electric field, the molecules in the upper region move to the left side, while the molecules in the lower region move to the right side. This confirms that the application of an electric field induces a backflow.

For further analysis, the computational domain was divided into ten subdomains in the vertical direction y^*. By taking averages of various variables over the molecules in the subdomains at time t^*, we obtained the instantaneous average velocity and orientation profiles as plotted in Fig. 3. The profiles of the horizontal component of velocity u^* confirm the transient "S-shaped" velocity profiles obtained in the calculation using continuum mechanics as reported in Ref. 1. Along with the change in molecular orientation, the magnitude of the velocity increases until a maximum value is

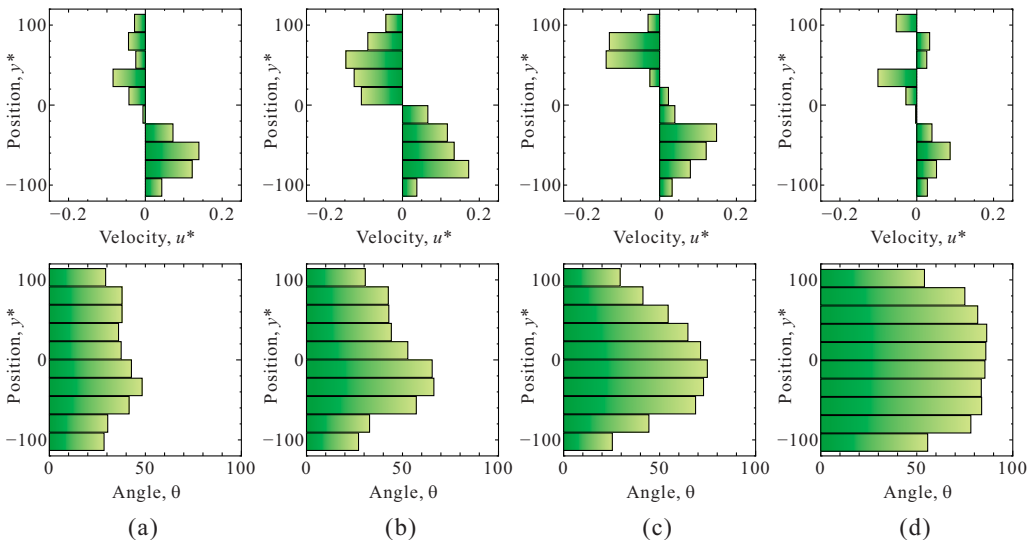

FIG. 3. (Color online) Profiles of horizontal velocity u^* (upper) and orientation angle θ (lower) after application of electric field for time $t^*=140$ (a), $t^*=240$ (b), $t^*=340$ (c), and $t^*=1000$ (d).

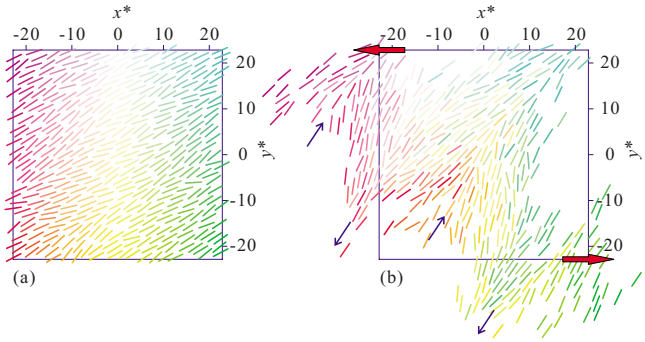

FIG. 4. (Color online) Close-up views of molecules at the center region at equilibrium (a) and after application of electric field for time $t^*=240$ (b).

reached, and then it decreases with increasing time t^*.

To investigate the roles of intermolecular interaction in the generation of bulk flow, close-up views of molecules in the center regions are shown in Fig. 4. For clarity, only the molecules that are initially located within the bounding box of Fig. 4(a) are shown in Fig. 4(b). The colors represent the initial positions of the molecules [Fig. 4(a)]. As shown in Fig. 4(b), after the application of the electric field, most of the molecules in the upper region move to the left, while those in the lower region move to the right (red arrows). Furthermore, there is a relative sliding motion parallel to the average direction of the molecules (blue arrows).

Figure 5 shows the molecular (a) and averaged (b) velocity vector in the center region after the application of the electric field for $t^*=240$. The average velocity vectors are obtained by dividing the simulation domain into 10×10 subdomains and averaging the velocities of the molecules in the subdomains. For clarity, the vectors in Fig. 5(b) are drawn 40 times larger than those in Fig. 5(a). Even though molecular velocities are apparently random, relatively ordered velocity vectors can be obtained by averaging. The average velocity vectors show the generation of a local bulk velocity gradient.

Mechanism of the generation of a bulk velocity gradient is illustrated in Fig. 6. The application of an electric field generates a torque that rotates the molecules such that their orientations are nearly parallel to the electric field direction.

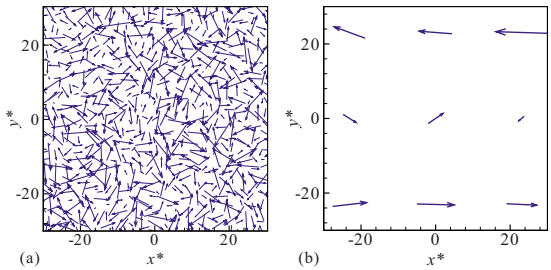

FIG. 5. (Color online) Molecular (a) and averaged (b) velocity vectors in the center region at time $t^*=240$.

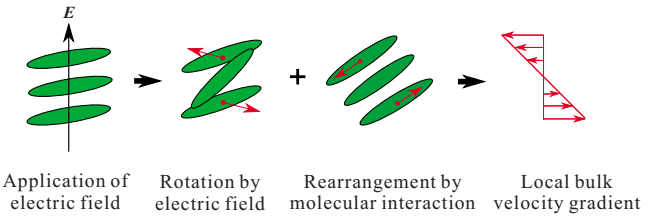

FIG. 6. (Color online) Generation of a bulk velocity gradient during the reorientation of molecules under the effect of an electric field.

When a molecule rotates faster than its adjacent molecules, it kicks the adjacent molecules such that the upper molecule moves in the upper-left direction, while the lower molecule moves in the lower-right direction. However, the interaction of the adjacent molecules with all other molecules forces them to rearrange themselves such that the potential energy remains minimal. This results in a slight reorientation of the molecules and a relative sliding motion, as confirmed in Fig. 4(b). On average, the rotation and rearrangement of the molecules result in the local bulk velocity gradient as confirmed in Fig. 5(b). With the presence of fixed walls, the local velocity gradients vary along the y^* direction. As proposed in Ref. 1, the integration of the local velocity gradients with appropriate boundary conditions would result in the S-shaped velocity profiles.

In summary, the mechanism of backflow generation has been investigated by molecular dynamics simulation. It was confirmed that the reorientation of molecules induces a transient velocity field. The rotation and rearrangement of molecules during the reorientation generate a local bulk velocity gradient, which is responsible for the generation of the bulk velocity field.

This work was partially supported by the Japan Society for the Promotion of Science through the Grant-in-Aid for Scientific Research for Young Scientists (Start-up).

[1] S. Chono and T. Tsuji, Appl. Phys. Lett. **92**, 051905 (2008).
[2] Y. Mieda and K. Furutani, Appl. Phys. Lett. **86**, 101901 (2005).
[3] F. Brochard, Mol. Cryst. Liq. Cryst. **23**, 51 (1973).
[4] C. Z. van Doorn, J. Appl. Phys. **46**, 3738 (1975).
[5] D. W. Berreman, J. Appl. Phys. **46**, 3746 (1975).
[6] J. L. Ericksen, Arch. Ration. Mech. Anal. **4**, 231 (1960).
[7] J. L. Ericksen, Trans. Soc. Rheol. **5**, 23 (1961).
[8] F. M. Leslie, Arch. Ration. Mech. Anal. **28**, 265 (1968).
[9] D. Marenduzzo, E. Orlandini, and J. M. Yeomans, Europhys. Lett. **71**, 604 (2005).
[10] A. N. Beris and B. J. Edwards, *Thermodynamics of Flowing Systems* (Oxford University Press, Oxford, 1994).
[11] J. G. Gay and B. J. Berne, J. Chem. Phys. **74**, 3316 (1981).
[12] P. Tian, D. Bedrov, G. D. Smith, M. Glaser, and J. E. Maclennan, J. Chem. Phys. **117**, 9452 (2002).
[13] R. Berardi, L. Muccioli, and C. Zannoni, J. Chem. Phys. **128**, 024905 (2008).
[14] M. Houssa, L. F. Rull, and S. C. McGrother, J. Chem. Phys. **109**, 9529 (1998).